CHAPTER 4

DESIGN METHODOLOGY, OPTIMIZATION AND BEAM-WAVE* INTERACTION SIMULATION OF A SECOND HARMONIC D-BAND GYROKLYSTRON AMPLIFIER

*Part of this work has been published as:

M. V. Swati, M. S. Chauhan, and P. K. Jain, "Design Methodology and Beam–Wave Interaction Study of a Second Harmonic D-Band Gyroklystron Amplifier," *IEEE Transactions on Plasma Science*, vol. 44, no. 11, pp. 2844-2851, 2016.

CHAPTER 4

DESIGN METHODOLOGY, OPTIMIZATION AND BEAM-WAVE INTERACTION SIMULATION OF A SECOND HARMONIC D-BAND GYROKLYSTRON AMPLIFIER

4.1. Introduction

The gyroklystron amplifier guarantees high gain per cavity and stability against oscillations that were not certain in other amplifying devices such as the gyro-TWT. The gain of the signal depends upon the number of cavities used with approximately a gain of 10dB per cavity. The main challenge in the performance improvement of gyroklystron is to obtain a high gain-bandwidth product in a device of low beam current and voltage. The choice of higher frequency and higher harmonic gyroklystron design is motivated by the requirement of higher power for specific applications at reduced magnetic field. But one of the major issues that affect the gyroklystron efficiency at higher frequencies and higher harmonics is the dense mode spectrum which affects the available operating mode. Thus, keeping all the factors discussed above into consideration, the purpose of the present chapter is to identify important parameters for the design of high frequency gyroklystron amplifier and to develop a suitable device design methodology. Further, the self-consistent multimode nonlinear formulation and simulation of the device is carried out to investigate the performance of the device due to mode competition. The second harmonic gyroklystron amplifier that can generate peak power in kilo-Watts at D-band (110 - 170GHz) is not yet reported to the best of our knowledge as per the literature review. The present work demonstrates the conceptual design methodology, a systematic design of a 140GHz, 1kW

second harmonic four-cavity gyroklystron amplifier with gain ~30dB which can be used in spectrometers for Electron Paramagnetic Resonance (EPR) experiments. Further, the multimode behavior of the device is studied with the help of commercially available 3D simulation code "CST Particle Studio" and is validated with the time-dependent multimode analysis as described in chapter 2.

This chapter of the thesis is organized as follows. In Section 4.2, the basic design methodology to the gyroklystron amplifier and its various design constraints are discussed. In Section 4.3, the multimode analysis of the designed gyroklystron amplifier is carried out to investigate its multimode beam-wave interaction behavior. Section 4 deals with the modeling of the RF interaction circuit of the gyroklystron amplifier in detail and the multimode beam-wave interaction behavior in a gyroklystron amplifier are investigated through the simulated results. Further, the validation of the simulated results with the analytical results is discussed in Section 4.5. Also, the sensitivity of the RF output power, efficiency and gain on the various device parameters are discussed in the Section 4.6. The main conclusions are drawn in Section 4.7.

4.2. Design Methodology

The design of the gyroklystron amplifier is more rigorous at higher frequencies, and at higher cyclotron harmonics (s >1) operation. Proper designing of the RF interaction structure is required because it ensures the device operation in the desired mode ahead of other parasitic competing modes. The initial mode selection process is done thoroughly by the design goals in terms of operating frequency, output power, and efficiency. The beam current and the beam voltage are initially chosen through the estimation of the desired output power, interaction efficiency, and the space charge effects. After the selection of

suitable operating mode, the beam parameters (i. e., beam guiding radius, velocity ratio), magnetic field and cavity radius is determined using the well established analysis [Kartikeyan *et al.* (2004), Nusinovich (2004)].

If the device is operating in the TE_{ml} mode at frequency f, the cavity wall radius (R_w) is evaluated by the expression [Nusinovich (2004)]:

$$R_w = \left(x'_{m_n l_n} \, c / 2\pi f \right) \ . \tag{4.1}$$

The optimum electron beam radius is given by [Nusinovich (2004)]:

$$R_b = \left(x'_{m_n \pm s,i} R_w / x'_{m_n l_n} \right) = \left(x'_{m_n \pm s,i} c / 2\pi f \right) \ , \tag{4.2}$$

where, x'_{ml} is the eigenvalue of the chosen mode, i is the radial beam position, which can be 1 or 2, and s is the harmonic number. The general expression of magnetic field strength (in T) at center of cavity for particular frequency is given by:

$$B_0 = \frac{f(GHz)\gamma}{28s} \ , \tag{4.3}$$

where, s is the harmonic number. Further, start oscillation current is investigated as a function of magnetic field to confirm the stable operation of the device. This calculation is computed for each cavity to fix the cavity length and to attain proper phase bunching. To maximize the electronic efficiency, the length of the drift tube

is to be optimized; with at least 40dB isolation between the two cavities [Chu *et al*. (1985), Chauhan *et al*. (2015)]:

$$L_d \ > \ \frac{4.6}{\left(\frac{x'_{m_n l_n}}{R_d} \right)^2 - \left(\frac{\omega_0}{c} \right)^2} \ , \tag{4.4}$$

where, L_d is the drift tube length. To minimize the cross talk between the cavities, the drift tube radius (R_d) should be small enough such that the operating mode is cut-off in this region; at the same time it should not obstruct the electron beam with guiding center R_b. Thus, the selection of drift tube radius should follow the condition:

$$R_b < R_d < R_w$$

The basic steps for designing the gyroklystron amplifier are summarized as follows:

1) Depending on the application, the operating frequency and the RF output power has to be determined. The designing of a gyroklystron amplifier initiates with the choice of the desired RF operating mode. Depending on the selected operating mode; the RF interaction structure parameters, electron beam parameter, and required DC magnetic field are evaluated. The finalization of the RF interaction structure consists of several steps. First, the resonance frequency and quality factor with a desired field profile of each cavity are chosen. Based on this information, cavities shapes, sizes and connecting drift tube radii are chosen.

2) The mode selection criterion includes the calculation of the coupling coefficient parameter and main design constraints namely wall losses, voltage depression, and limiting current. The coupling coefficient parameter determines the coupling of the electron beam to the RF mode in the cavities. The coupling coefficient curves help us to decide the optimum beam radius for maximum beam to mode coupling so that the operating mode is excited and other competing modes are suppressed. Proper mode selection ensures that the design constraints are within the limits.

3) For the investigation of stable operation of a gyroklystron amplifier, the start oscillation current criteria study is necessary. Since gyroklystron is an amplifier, therefore,

its operating current value is chosen such that it should be always less than the start oscillation current. The start oscillation current is calculated for all the possible nearby modes to ensure the device operating condition in the desired mode with maximum efficiency. The beam current and the magnetic field are mainly decided by the start oscillation current criteria study.

4) The various device input parameters, such as beam voltage, beam current, transverse to axial beam velocity ratio (pitch factor), guiding center radius, and magnetic field values are judiciously chosen with the help of its parametric analysis to achieve the desired efficiency and output power.

5) The space charge effect can be defined in terms of the voltage depression (V_d) and the limiting current (I_L). For the effective operation of a gyroklystron amplifier, the voltage depression is likely to be small and the limiting current should be as high as possible.

6) The number of cavities and their dimensions are chosen based on the nonlinear theory.

7) The cavity circuit is then modeled and optimized using the simulation tool "CST particle Studio".

4.2.1. Mode Selection

For the device operation at the specific frequency, it is necessary that the device should work in that particular mode. Device operation in the parasitic modes results in the shift in its operating frequency and also results in the decrease in the efficiency. In order to ensure the excitation of the desired mode, various factors have to be considered in a gyroklystron amplifier. To accommodate the large peak power, all the cavities of gyroklystron amplifier should be designed for stable operation in the desired mode. The cavity radius needs only to be large enough to support the desired mode. Thus, proper

mode selection is an important criterion for the successful design of the gyroklystron amplifier. It depends on several design constraints, such as, coupling efficiency, ohmic losses, voltage depression, and limiting current.

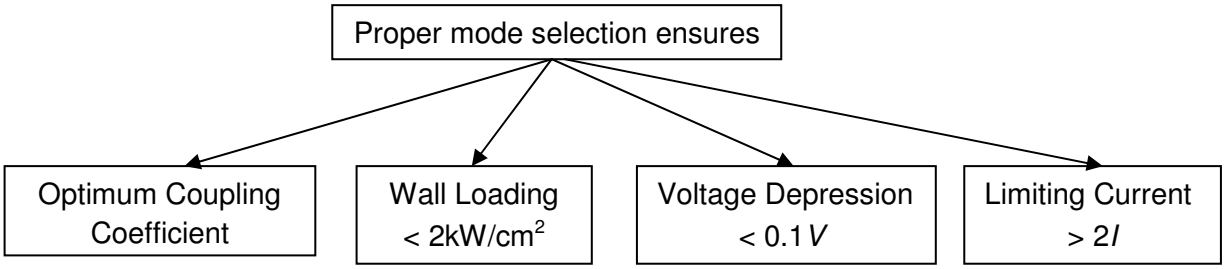

Table. 4.1: Design goals.

Parameters	Specifications
Beam Voltage (V_b)	~40kV
Beam Current (I_b)	~1A
Velocity Pitch Factor (α)	1.4 - 1.5
DC Magnetic Field (B_0)	2.6 - 2.8T
Drive Frequency	140GHz
RF Output Power	~1kW

4.2.1a Coupling coefficient

The beam-wave coupling coefficient is one of the major parameter for the mode selection. Coupling coefficient gives the information regarding selection of beam radius for the maximum coupling in the desired mode so that the desired mode can be excited properly during the device operation. It also gives information regarding the electric field distribution for a particular mode. Once the desired mode is coupled properly by the electron beam, other competing modes are suppressed and the device is leading to the single-mode stability.

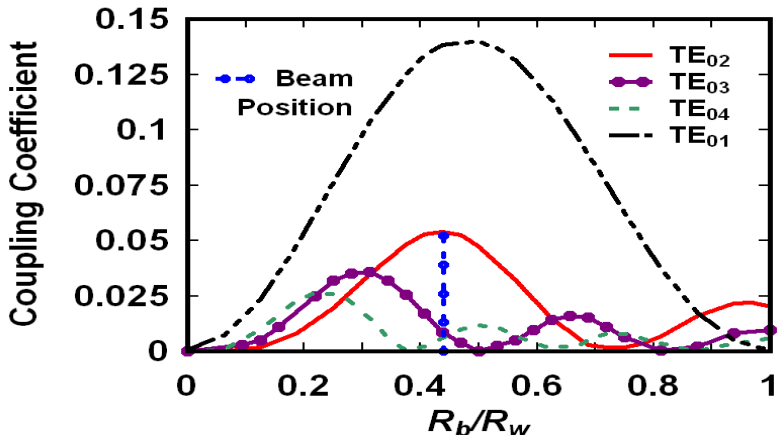

Figure. 4.1: Coupling coefficient as a function of ratio of beam to waveguide radii (R_b/R_w) for the different modes.

The coupling coefficient between the electron beam and the RF fields in the cylindrical cavities is defined as [Tran *et al*. (1986)]:

$$H_{m_n l_n} = \frac{J^2_{m_n \pm s}\{k_{nt} R_b\}}{(x'^2_{m_n l_n} - m_n^2) J^2_{m_n}\left\{x'_{m_n l_n}\right\}}\ , \tag{4.5}$$

where, $k_\perp = 2\pi/\lambda$, R_b is the beam radius, $x'_{m_n l_n}$ is the eigenvalue of the n^{th} TE_{ml} mode. Figure 4.1 shows the dependence of the coupling coefficient on the electrons guiding center radius for the azimuthally symmetric modes. In terms of the coupling between the electron beam and the RF waves, the fundamental mode, i. e., TE_{01} is the most suitable mode for operation. However, at higher frequency of operation, the TE_{01} mode facilitates a smaller cavity radius due to reduced transverse dimensions which in turn increases the ohmic wall heating. To minimize the ohmic wall losses, higher order modes, such as, TE_{03} or TE_{04} can be used, but at the cost of reduction in coupling efficiency. Hence, a lower order mode, i. e., TE_{02} mode is chosen as the operating mode in each cavity to ensure the benefits of high coupling coefficient, lower wall losses, feasible cathode design, and an easier design of

mode convertors. The first radial maximum of TE_{02} mode, i. e., $R_b/R_w = 0.44$, is selected as normalized beam position for optimum coupling between the electron beam and RF wave.

4.2.1b Wall loading

Another consideration in choosing the mode of operation is ohmic heating of the cavity walls. In the relatively low power systems, such as in the present case, ohmic wall heating is quite small, and hence wall loading is not a serious issue. The ohmic wall losses, which mainly occurs because of the cavity wall heating, due to the finite conductivity of the cavity material, is one of the important design constraint for the output cavity and can be computed as [Kreischer *et al*. (1985)]:

$$\rho_{ohm} = \frac{1}{2\sigma\delta}\left|\hat{n}\times H\right|^2_{r=R_b} = \frac{1}{2\sigma\delta\mu_0^2}\left(1+\frac{m^2k_z^2}{k_{ml}^4R_b^2}\right)\frac{k_{ml}^2}{\omega^2}E_0^2J_m^2\left\{k_{ml}R_b\right\}\left|f\left\{z\right\}\right|^2 \quad , \tag{4.6}$$

where, δ is the skin depth, σ is the electrical conductivity of the cavity wall. The second term in the bracket is negligible in the cutoff limit $k_z << k_{ml}$. This expression of ohmic loss density can be expressed in terms of the normalized parameters F, μ, and Δ as [Kreischer *et al*. (1985)],

$$\rho_{ohm}(W/m^2) = 5.1\times10^{-15}\sigma^{-0.5}\omega^{2.5}F^2\beta_t^6C_t^2\gamma^2(1-0.5\beta_t^2\Delta)^2 \quad , \tag{4.7}$$

where, $C_t = \dfrac{J_m\left\{x'_{ml}\right\}}{J_{m\pm s}\left\{k_{ml}R_b\right\}}$. This will provide the choice of the cathode voltage and field amplitude for a tolerable wall loss. For a Gaussian axial profile function, $f\left\{z\right\} = \exp(-4z^2/L^2)$, the stored energy in the cavity is:

$$U_w = \varepsilon_0E_0^2\left(\frac{\pi}{2}\right)^{3/2}\frac{L}{2k_{ml}^2}\left(x'^2_{ml}-m^2\right)J_m^2\left\{x'_{ml}\right\} \ . \tag{4.8}$$

Using, $$Q_D \equiv \frac{\omega U_w}{P}, \tag{4.9}$$

where, Q_D is the diffractive quality factor, P is the power flow from the output end of the cavity, and combining equations (4.6) and (4.8), the equation relating the cavity mode indices to the ohmic loss density for a given output power is as:

$$\left(x'^{2}_{ml} - m^2\right) = \frac{16\pi}{c^3}\sqrt{\frac{2}{\sigma\mu_0}}\left(\frac{L}{\lambda}\right)\frac{Pf^{5/2}}{(1-R_2)\rho_{ohm}}$$

$$= 1.05\times10^{-3}\left(\frac{L}{\lambda}\right)\frac{P(MW)f^{5/2}(GHz)}{(1-R_2)\rho_{ohm}(kW/cm^2)} \quad . \tag{4.10}$$

The maximum wall losses can be estimated from:

$$\left(\frac{dP}{dA}\right)_{\max} \approx \sqrt{\frac{8}{\pi}}\sqrt{\frac{1}{\pi Z_0\sigma}}\frac{PQ}{L\lambda^{1.5}}\frac{1}{x'^{2}_{ml} - m^2} \quad . \tag{4.11}$$

Thus, from equation (4.11) it is clear that the maximum wall loss can be controlled by lowering the output cavity quality factor. In simulations, the Q-factor can be lowered by directly lowering the conductivity of the copper material. But in practical conditions, the copper conductivity cannot be changed; rather the Q-factor is lowered by loading the cavities with lossy ceramic material or by cutting the leaky slots in the cavity walls. It is desired to keep the maximum wall losses at a level below 2.0kW/cm^2. For the RF output power of ~1kW and output cavity quality factor of 600 (as considered in the present design), the wall losses for the selected TE_{02} mode is obtained as ~0.24kW/cm^2, which is well within the limit i. e 2kW/cm^2.

4.2.1c Voltage depression and Limiting current

Another important consideration in the design process is the space charge effect which is a common phenomenon that occurs due to the potential of the transported charged beam and plays a vital role in the beam quality in the interaction region. The space charge

effect of gyrating beam is defined in terms of voltage depression (V_D) and limiting current (I_L). Due to the presence of the space charge of the electron beam, a negative potential of the electron beam is created which screens the electrons partially from the applied accelerating cathode voltage. The difference between the accelerating cathode voltage (V_k) and the corresponding beam voltage (V_b) describes the voltage drop also known as voltage depression within the hollow electron beam w. r. t. cavity wall. Due to this potential drop, applied accelerating voltage is not fully available to the beam and can also change the resonance condition in the interaction cavity. The limiting current is the current for which the voltage depression becomes so large that the beam cannot propagate (the normalized axial velocity component of the electron beam becomes zero and the mirroring of the beam occurs). However, in the case of a gyroklystron amplifier, the operating current is well below the limiting current. As, for the stable operation of a gyroklystron as an amplifier, the necessary condition for beam current is $I_b < I_{st} < I_L$, but the space charge effects due to voltage depression may still be significant. The upper limit for the voltage depression is roughly estimated to be around 10% of the applied beam voltage, and the cutoff point of the limiting current is around twice the operating beam current.

The effect of voltage depression can be reduced to an extent by increasing the beam voltage, and by making use of depressed collector [Chu *et al.* (1985), Ganguly *et al.* (1984), Kartikeyan *et al.* (2004)]. The voltage depression (V_D) and the limiting current (I_L) can be mathematically expressed as follows [Ganguly and Chu (1984), Kartikeyan *et al*. (2004)]:

$$V_D \approx 60 \frac{I_b}{\beta_{\parallel}} \ln\left(\frac{R_w}{R_b}\right) \quad , \tag{4.12}$$

and $$I_L \approx 8500A\left[\gamma^* / \ln\left(\frac{R_w}{R_b}\right)\right] \quad , \tag{4.13}$$

where, $\gamma^* = \gamma_0\left[1-\left(1-\beta_{\|0}^2\right)^{1/3}\right]^{3/2}$, I_b is the beam current, $\beta_{\|0}$ is the value of $\beta_{\|}$, and γ_0 is the relativistic factor at the inlet of the input cavity respectively.

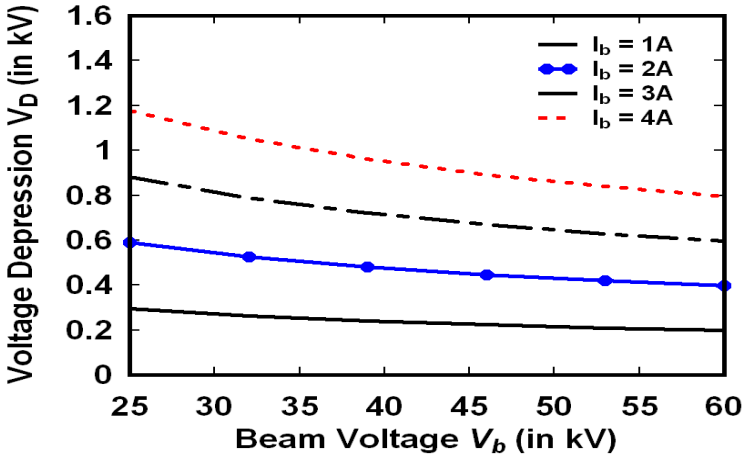

Figure. 4.2: Dependence of voltage depression on beam voltage for different values of beam current.

From equations (4.12) and (4.13), it is clear that the voltage depression and limiting current depend mainly on the beam radius and the cavity wall radius. Moreover, from equations (4.1) and (4.2), it is evident that the beam radius and the cavity radius are selected on the basis of operating mode and thus, the space charge effect in the interaction cavities can be easily controlled by making a proper choice of operating mode.

Figure 4.2 shows the dependence of voltage depression on the beam voltage for different values of beam current. It is quite evident from Fig. 4.2, that at the high beam current operation, voltage depression increases, which results in the reduction of device efficiency due to the potential drop and beam energy spread effects caused by the voltage depression.

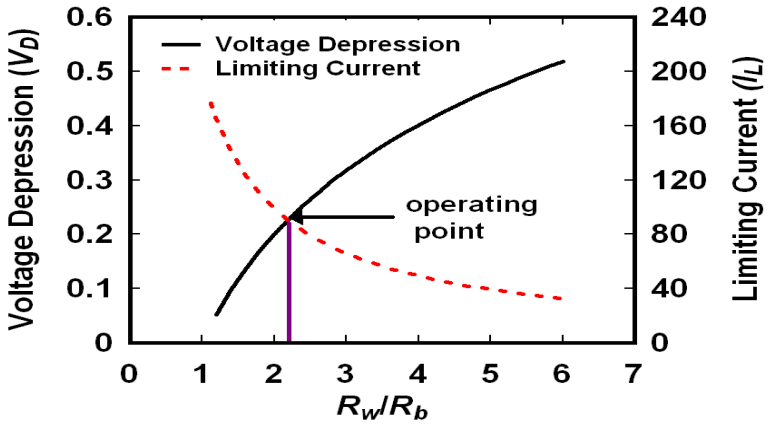

Figure. 4.3: Voltage depression and limiting current versus the ratio of waveguide to beam radii (R_w/R_b).

Figure 4.3 shows the voltage depression and the limiting current variation respectively as a function of the cavity wall to the electron beam radii ratio (R_w / R_b). The voltage depression increases with R_w / R_b, while the limiting current decreases. For the chosen operating point, i. e., $R_w / R_b = 2.27$, voltage depression is obtained as ~0.24kV whereas the value of limiting current is ~ 90A. It means for the chosen TE_{02} mode; the space charge effects are within the limits for selected input beam parameters of 40kV beam voltage and 1A beam current.

4.2.2. Start Oscillation Current

Since in gyro-devices, the modes which are in cyclotron resonance with the electrons can be excited, hence this allows providing the mode selection by proper choice of the magnetic field. The study of start oscillation current criteria helps to estimate the desired magnetic field. The start oscillation current is current at which cavity starts oscillating even in the absence of driver signal. For the efficient operation of gyroklystron as an amplifier, it is necessary that the operating current should be less than the start oscillation current which depends on the beam properties, cavity dimensions, cavity Q's and the DC magnetic field. Thus, for the stable operation, information of the start oscillation current (I_{st}) of the device as a function of the magnetic field is necessary.

The general expression of magnetic field strength (in Tesla) at the center of cavity for particular frequency is given by the equation (4.3). For operating frequency of 140GHz and second harmonic operation (s = 2), the DC magnetic field is obtained around 2.695T. The obtained magnetic field is further optimized using start oscillation criteria study for the stability of the device. It is also important to estimate the start oscillation current of various possible competing modes. By calculating and comparing the start oscillation current of desired and competing modes, it is ensured that the required mode is excited with maximum efficiency at the desired power level, thus suppressing the unwanted modes. Considering the Gaussian profile at the output cavity, the normalized start oscillation current in terms of the normalized interaction length of the cavity μ, and detuning parameter Δ is given by [Fliflet *et al.* (1982), Gold *et al.* (1990)]:

$$\hat{I}_{st}(\mu,\Delta) = (4/\pi\mu^2)[e^{2x^2}/(\mu x - s)] \quad , \tag{4.14}$$

where, $x = \mu\Delta/4$. Actual start oscillation current is calculated by putting the normalized beam current equal to the normalized start oscillation current and is thus given by:

$$I_{start} = \left(\frac{\pi}{2}\right)^{5/2} \frac{c^3 m_e \varepsilon_0}{e} \left(\frac{2^s s!}{s^s}\right) \frac{\beta_{\perp 0}^{-2(3-s)} \gamma_0}{Q} \frac{L}{\lambda} \frac{(4/\pi\mu^2)[e^{2x^2}/(\mu x - s)]}{H_{m_n l_n}} \quad . \tag{4.15}$$

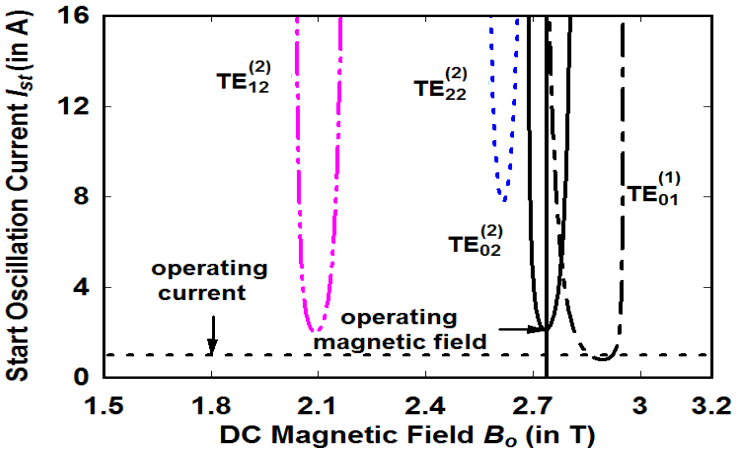

Figure. 4.4: Start oscillation current I_{st} for second harmonic TE_{02} mode and other possible competing modes as a function of DC magnetic field at the output cavity.

Figure 4.4 shows the plot of the start oscillation current with respect to DC magnetic field B_0 for the operating mode ($TE_{02}^{(2)}$) and the nearby possible competing modes in a 140GHz, second harmonic gyroklystron amplifier. It can be observed that, by choosing the DC magnetic field of around 2.74T, the start oscillation current for the $TE_{02}^{(2)}$ mode in the input cavity is obtained as ~3A. Hence, the cavity is stable for any operating current values chosen below the start oscillation current. The operating current is selected as 1A for the present design. It is observed that the nearby competing modes $TE_{22}^{(2)}$, $TE_{12}^{(2)}$, and $TE_{01}^{(1)}$ are also not oscillated as the operating current is below the start oscillation current for the chosen magnetic field.

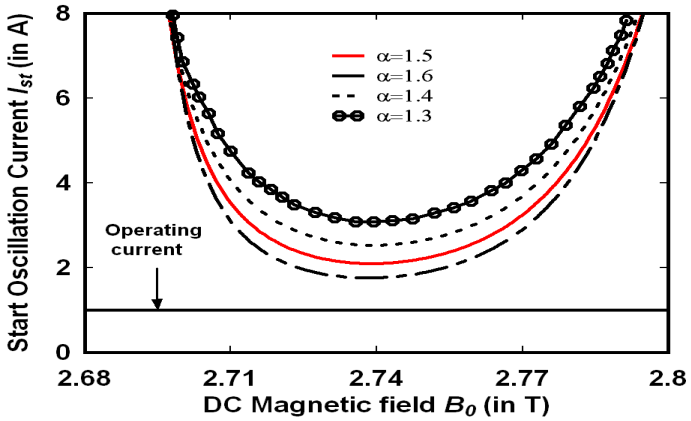

Figure. 4.5: Start oscillation current I_{st} as a function of DC magnetic field at the output cavity for different values of beam pitch factor.

Figure 4.5 shows the effect of electron beam pitch factor (α) on the stability of the operating TE_{02} mode in the output cavity. It is clear from the figure that with the increase in α, the stability of the RF cavity decreases due to the decrease in the start oscillation current values. For the stability of the device and for obtaining desired output power, the beam pitch factor is chosen to be 1.5.

Table. 4.2: Specifications for 140GHz, 1kW second harmonic four-cavity gyroklystron.

Parameter	Radius (in mm)	Length (in mm)	Quality factor
Input Cavity	2.413	8	300
Buncher Cavity	2.409	9	500
Penultimate Cavity	2.415	8	500
Output Cavity	2.396	9.71	600
Input-Buncher Drift Tube	1.735	25	-
Buncher-Penultimate Drift Tube	1.735	20	-
Penultimate-Output Drift Tube	1.735	10	-
Up-taper	3.98	38.36	-

Table. 4.3: System parameters.

Parameter	Specifications
Beam Voltage	40kV
Beam Current	1A
Pitch Factor	1.5
Axial Magnetic Field	2.74T

Table 4.2 and Table 4.3 show the optimized design parameters and the system parameters for the designed gyroklystron amplifier. Thus, for a 140GHz, four-cavity gyroklystron, the initial input parameter is fixed on the basis of the required RF output power (~ 1kW), efficiency (~ 3%) and gain (~ 30dB). The design values obtained by adapting the present methodology are used as input parameters for the beam-wave interaction behavior study through time-dependent multimode nonlinear analysis as described in Chapter 2. The efficiency and RF output power of the device is estimated using (2.66) and parameters are optimized for the optimum performance in terms of efficiency and RF output power.

4.3. Time-Dependent Nonlinear Multimode Analysis

The design parameter of a typically selected 140GHz second harmonic gyroklystron amplifier have been finalized based on the above discussed design methodology and are

shown in Table 4.2. For the design of a 140GHz, four-cavity gyroklystron amplifier having 1kW RF output power with 30dB gain, the initial input parameters are fixed on the basis of the required RF output power and the efficiency ~3%. The beam current and beam voltage are optimized using nonlinear analysis to get the desired RF output power and efficiency. The required values of quality factor in the cavity and the beam pitch factor are mainly decided by the stability condition of the device using start oscillation current criteria. In comparison to the experimental three-cavity second harmonic gyroklystron amplifier reported by [Antakov *et al.* (2011)], discussed in the previous chapters, the present gyroklystron amplifier is designed to be operated at higher frequency with higher efficiency and number of cavities is increased to four to obtain the desired gain. However, for high frequency operation of gyroklystron amplifier, it is a challenging task to avoid the mode competition. Hence, to study the effect of competing modes on the device performance and to observe the temporal growth of output power in all the modes, the time-dependent multimode nonlinear analysis of the device as described in chapter 2 has been carried out.

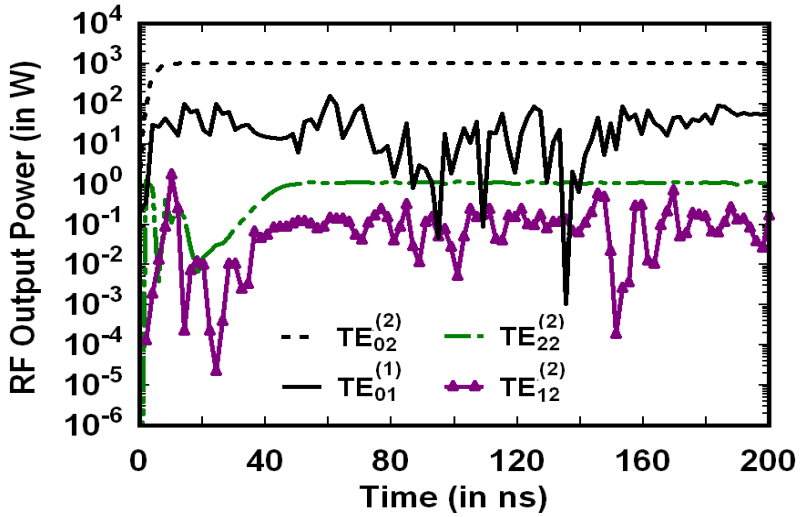

Figure. 4.6: Analytical temporal power growth obtained by developed multimode analysis for the operating second harmonic TE_{02} mode along with the possible competing modes (for $B_0 = 2.74$T and $P_{in} = 1$W).

Figure 4.6 shows the temporal growth of RF output power in the operating TE_{02} mode and the nearby competing modes obtained from the time-dependent multimode analysis for the designed parameters shown in Tables 4.2 and 4.3. It is clear from the figure that the saturated output power of ~1.03kW is obtained in the second harmonic TE_{02} mode and the fundamental harmonic TE_{01} mode. The saturated RF output power is obtained as ~100W in the fundamental TE_{01} mode. The device efficiency and gain are calculated as ~2.58% and ~30.13dB, respectively.

4.4. Device Simulation

The multimode beam-wave interaction analysis studied in the previous section is further validated through PIC simulation using "CST Particle Studio". The simulation process consists of mainly three steps. Firstly, the RF interaction structure of the device is modeled by taking into the account of the relevant device design parameters, as listed out in Table. 4.2. The beam-absent (cold) analysis is then performed to examine the electromagnetic behavior of the device, such as, the operating mode, frequency, field excitation, cavity quality factor, etc. As the last step, the device RF output performance evaluation is carried out in terms of RF output power, gain and bandwidth by simulating the device in the presence of the electron beam (hot analysis).

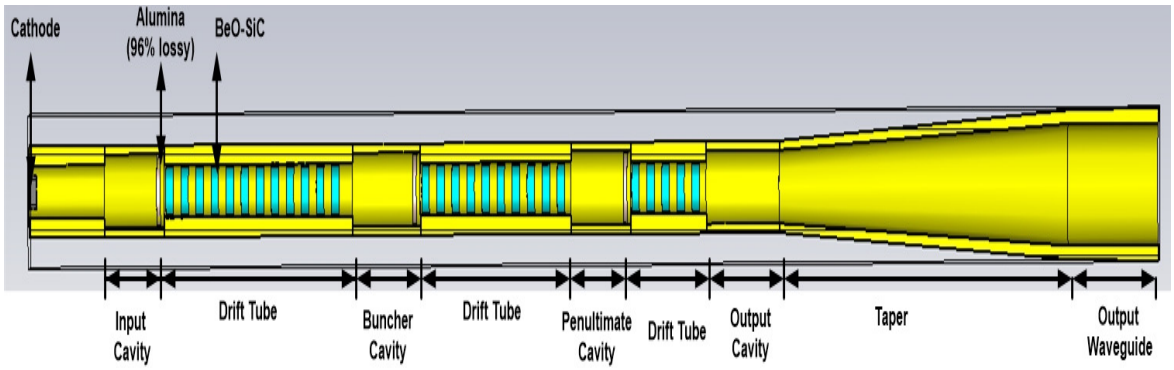

Figure. 4.7: Simulated view of the cross-section of the gyroklystron interaction circuit.

4.4.1. Modeling of the RF Interaction Structure

A 2D view of the RF interaction circuit of a four-cavity D-band second harmonic gyroklystron amplifier modeled in CST for PIC simulation is shown in Fig. 4.7. The RF interaction structure is modeled with copper material (conductivity σ =5.8 x 10^7 S/m) to reduce the ohmic losses, and the background is set as vacuum during simulation. Several other parameters are also accounted in the modeling of the RF interaction structure, like, the cavity radius, drift tube radius, resonating frequency, and the *Q*-factor. The *Q*-factor of the cavities should be adjusted to allow the device operation below the start oscillation current. To ensure the stability, the device should be operated below the start oscillation current. To achieve this, the *Q*-factor of the cavities should be adjusted. In simulations, the *Q*-factor of the cavities can be directly lowered by lowering the copper conductivity. But the procedure cannot be applied during the practical or real-time manufacturing due to the fixed conductivity of the copper material. In order to follow the real-time simulation process, the cavities are loaded with lossy dielectric ring of alumina at the sidewall of the cavity to achieve the optimized *Q*-factor. The *H*-field monitor is set for the *Q*-factor calculation. The drift tubes are externally loaded with lossy ceramic rings of BeO-SiC [Samartsev *et al.* (2011)] having complex permittivity as $\epsilon=15+j4$ at 140GHz to provide complete isolation between the adjacent cavities by absorbing the field leaked from cavities to drift region or should attenuate possible RF fields. The ceramic ring has 2mm length and the radial thickness is 1mm. It is a lossy material due to its good thermal conductivity and which is also important for high average power operation. By setting the phase space monitors, phase space for energy of electrons is recorded for analyzing the electron bunch and energy transfer phenomena. The *E*-field monitor is set to observe the fields inside the

RF cavity which ensures the cavity operation in the desired mode and frequency. A port is assigned at the end of the RF interaction structure to observe the RF output power. The input cavity has been excited in the desired mode corresponding to specific frequency and power with the help of a driver, i. e., a current-density source to drive electromagnetic fields in a local region of space.

4.4.2. RF Cavity Simulation (Beam Absent Condition) — Eigenmode Study

In order to confirm the device operation in the desired frequency and mode, the eigenmode simulation of the RF cavity is carried out in the absence of electron beam using eigenmode solver of 'CST Microwave studio'. The tangential component of the electric field becomes null at the metal boundary ($E_t = 0$). Using this technique, the presence of a particular mode inside the cavities is confirmed by observing the electric field pattern.

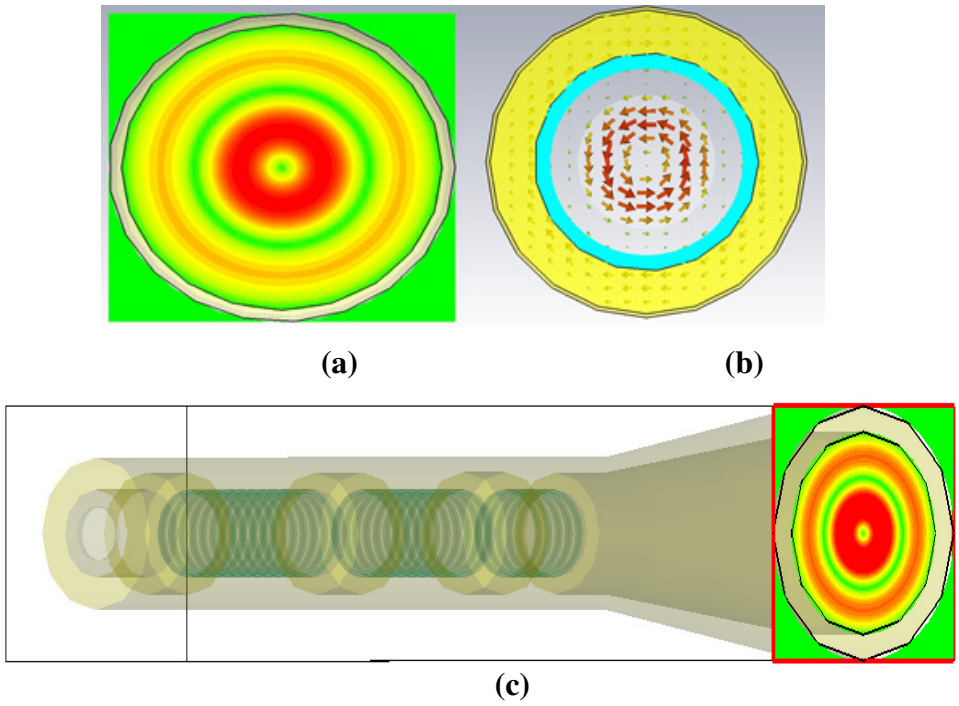

Figure. 4.8: Electric field pattern at the input cavity of gyroklystron: **(a)** Contour plot, **(b)** Vector plot and **(c)** Contour plot at the output port.

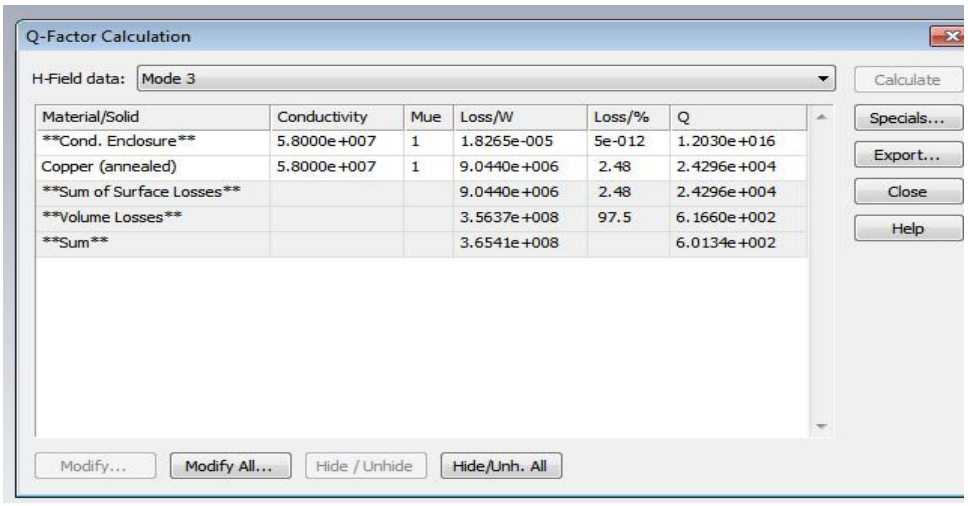

Figure. 4.9: Q-factor calculation in the output cavity.

Figure 4.8(a) and 4.8(b) shows the contour plot and vector plot of the electric field pattern inside the input cavity of gyroklystron amplifier. From the figure, it is clear that there is no variation in the azimuthal direction and two variations in the radial direction which confirms the TE_{02} mode of operation in the cavity. Figure 4.8(c) shows the contour plot at the output port of the gyroklystron amplifier which indicates that the same operating mode (TE_{02}) is coming out of the uptaper section after amplification. The loss calculation inside the cavity is accessible through 2D/3D field processing → Loss and Q calculation which includes the dielectric loss. As a result of this loss calculation, the Q factor of a cavity is available. Figure 4.9 shows the Q-factor calculation in the output cavity. It is clear from the figure that the Q is obtained as around 600 in the output cavity.

4.4.3. PIC Simulation of the RF Interaction Structure (Beam Present Condition) — Beam-Wave Interaction Study

After performing the beam-absent simulation, the simulation is extended for the beam-present case. Gyrating electron beam of 40kV beam voltage, 1A beam current having a pitch factor of 1.5 is applied at the input end of the interaction structure. Uniform

magnetic field of 2.74T is applied along the interaction length. Eight beamlets are taken in the structure for the simulation of beam wave interaction in the gyroklystron amplifier. However, these numbers of beamlets can be taken larger to have better results but, of course, on the cost of time and memory consuming.

The cross-section of the electron beam with 8 beamlets before and after the RF interaction are shown in Figs. 4.10(a) and 4.10(b). Figure 4.10(a) shows that before interaction, all the 8 beamlets are uniformly distributed with the fixed guiding center radius and their energies are equal at the starting of the interaction process. During the beam-wave interaction process, the electrons lose their energy and give their energy to RF, hence after some time electrons are not uniformly distributed and the bunching of electron particles lead to the change in their Larmor radius which is clearly shown in the Fig. 4.10(b).

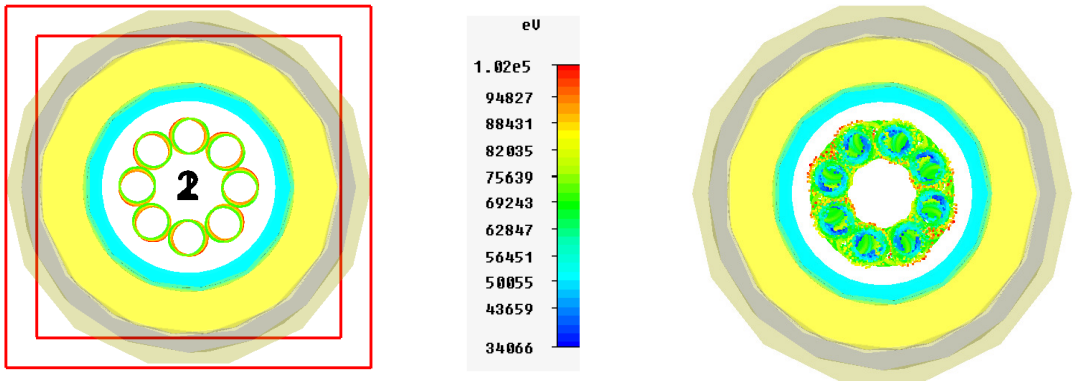

(a) **(b)**

Figure. 4.10: Front view of electron beam with 8 beamlets **(a)** before interaction **(b)** after interaction.

The contour plot of the electric field pattern of the TE_{02} mode along the axial length of the interaction circuit is shown in Fig. 4.11. At the input cavity, no propagation of the RF field is observed while the RF field amplitude gradually strengthens along the z-axis. It can be

seen that the RF field strongly resonates in the output cavity forming a standing wave while in the output taper, RF field is present forming a travelling wave.

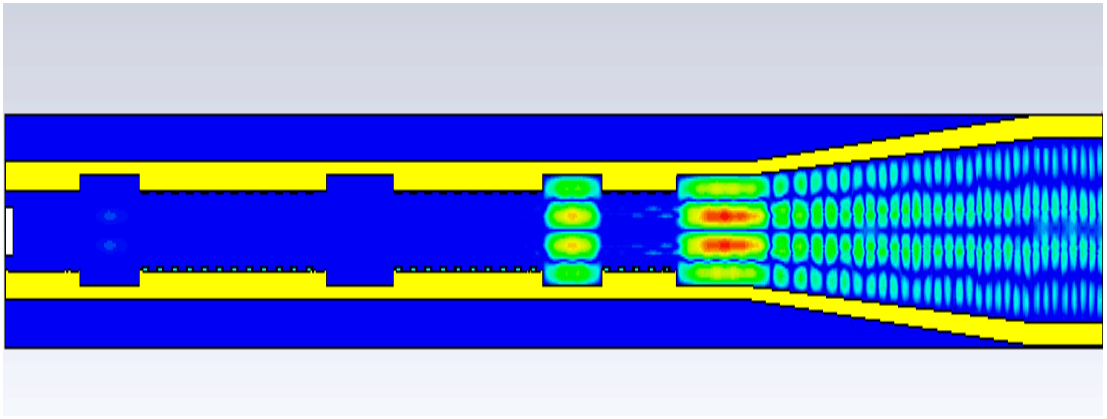

Figure. 4.11: Contour plot of the electric field pattern of TE_{02} mode along the axial length of interaction circuit.

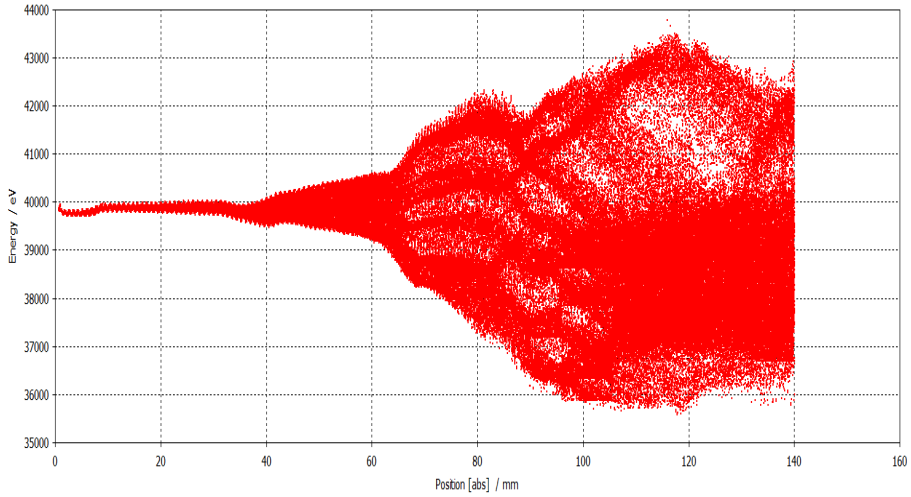

Figure. 4.12. Evolution of particle energy along the axial length of interaction circuit.

The evolution of electron energy along the interaction region is shown in Fig. 4.12. It can be seen that initially all the electrons have the same energy of 40keV but with time, the net energy of particles get perturbed along the cavity length due to the interaction with the RF field. At the output end of the cavity, majority of particles have lower energy which indicates the net energy transfer from the electrons to the RF wave, hence results in the

amplification of the RF wave. To determine the operating frequency of the gyroklystron amplifier, the frequency spectrum of the electric field amplitude is calculated which is obtained by taking the Fourier transform of the electric field (Fig. 4.13). It is clear from the figure that the highest frequency peak is observed at around 140GHz for second harmonic TE_{02} mode, hence confirms its frequency of operation.

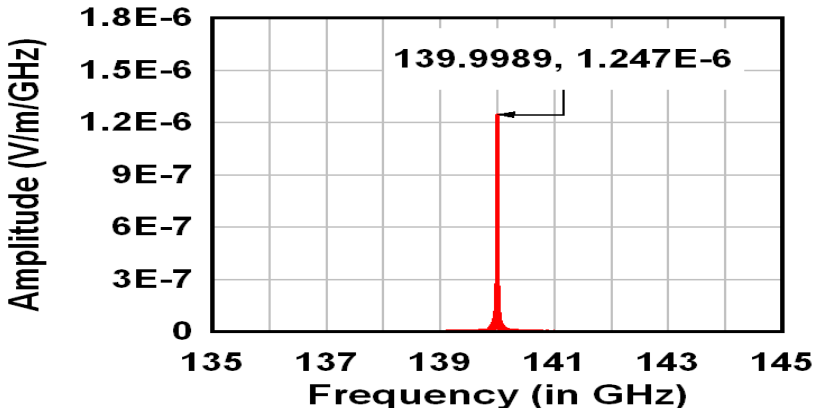

Figure. 4.13. Frequency spectrum of electric field amplitude to determine the operating frequency of gyroklystron amplifier.

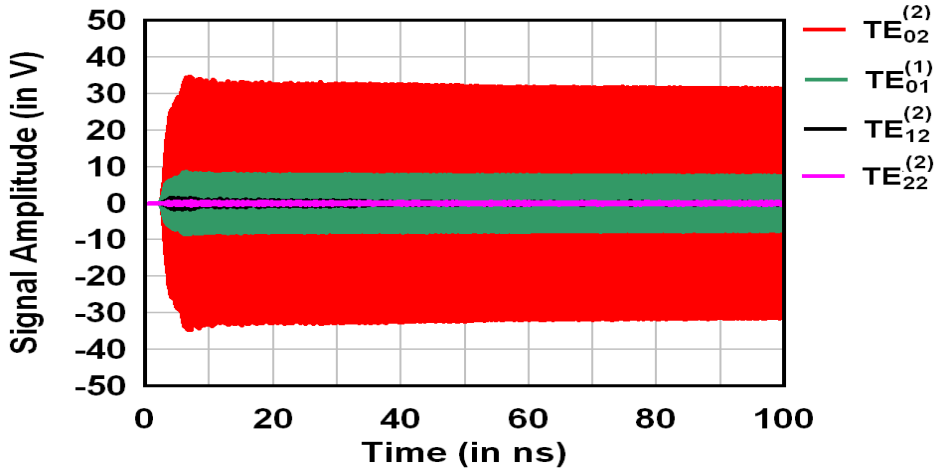

Figure. 4.14: Temporal growth of the EM signal in the operating $TE_{02}^{(2)}$ mode along with other competing modes.

The temporal growth of the field amplitude in the operating TE_{02} mode and the other nearby competing modes has been shown in Fig. 4.14. The output time signal corresponding to TE_{02} mode has the highest amplitude than all other modes at DC magnetic

field $B_0 = 2.74$T and mode competition is mainly observed due to the fundamental harmonic TE_{01} mode. The growth of EM power approaches saturation level at a time beyond 20ns.

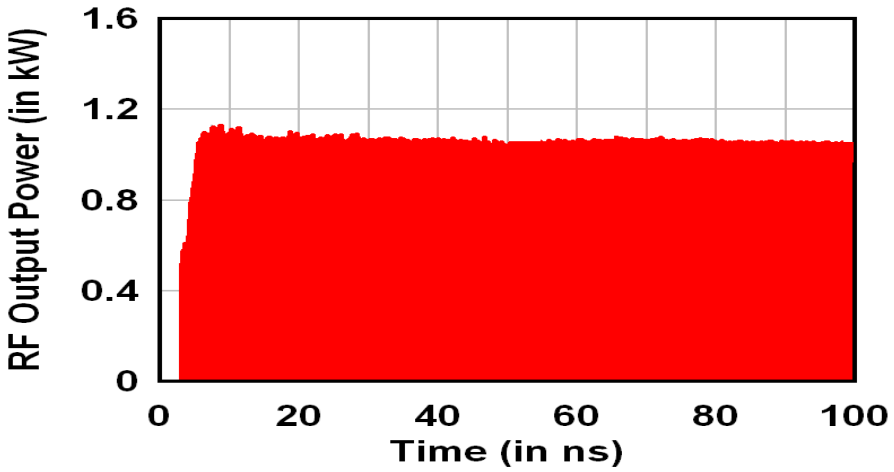

Figure. 4.15: PIC simulation plot for the temporal growth of the RF output power in the operating $TE_{02}^{(2)}$ mode.

After the template based post processing in CST particle studio, the saturated RF output power has been calculated as around 1.01kW with an electronic efficiency of 2.52% for 40kV, 1A annular electron beam with a velocity pitch factor of 1.5. The gain of the device has been obtained as around 30.04dB (Fig. 4.15).

4.5. Device Design and Simulation Validation

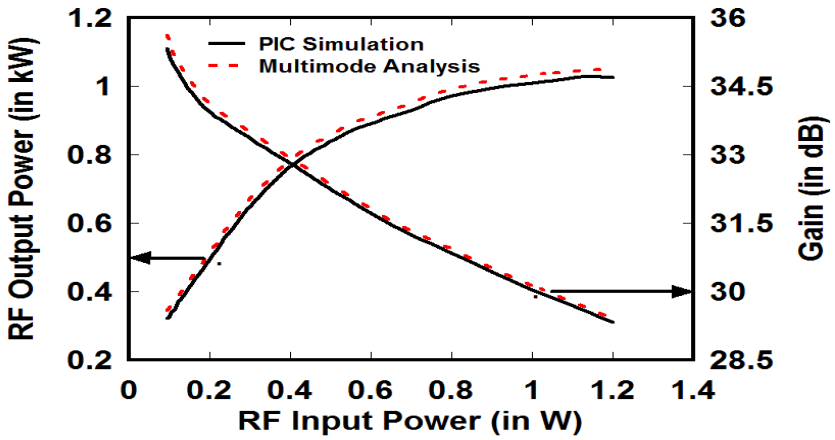

Figure. 4.16: RF output power and gain variation with input drive power (P_{in}) (V_b = 40kV, I_b = 1A, α = 1.5 and f_{dr} = 140GHz).

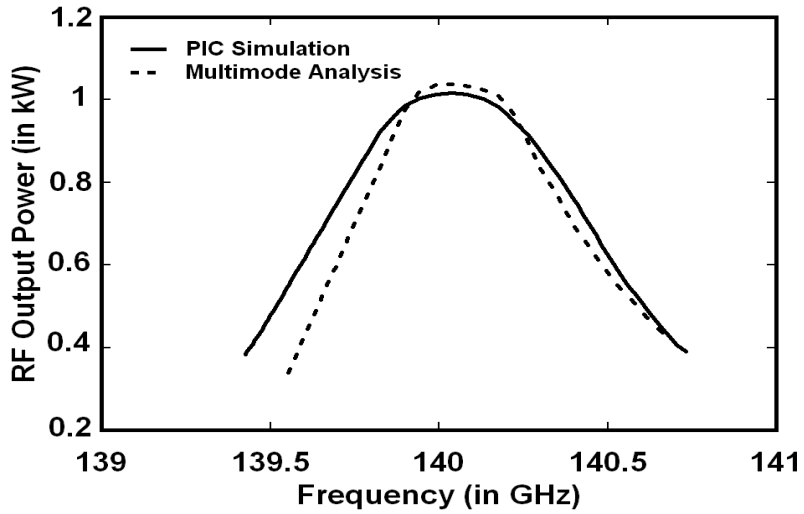

Figure. 4.17: Analytical and simulated RF output power variation with the driver frequency (V_b = 40kV, I_b = 1A, α = 1.5 and B_0 = 2.74T).

To validate the optimized gyroklystron design obtained by following the device design methodology, the PIC simulation results obtained by modeling the device through CST Particle Studio are validated with the analytical results obtained through the time-dependnt nonlinear multimode analysis.

Figure 4.16 shows the RF output power and gain as a function of RF input power for beam voltage corresponding to 40kV and beam current corresponding to 1A at 140GHz center frequency. It is clear from the figure that the RF output power increases rapidly with increasing input power when the input power is less than about 1.0W and then reaches saturated value around 1.03kW (gain ~30.04dB) in case of the PIC simulation and around 1.05kW (gain ~30.07dB) in case of analytical calculations. The results obtained from PIC simulation are validated with the time-dependent multimode analysis and are found to be in agreement. The 3dB bandwidth of the gyroklystron amplifier is obtained by observing the RF output power as a function of frequency (Fig. 4.17). It is evident from the figure that the designed gyroklystron amplifier achieved a 3dB bandwidth of 1080MHz and 917MHz from PIC simulation and multimode analysis, respectively. Bandwidth obtained from PIC

simulation has higher value as it considers the basics of stagger tuning i. e., all the cavities resonate at slightly different frequencies.

4.6. Parametric Analysis

To make the present study more practically useful, the parametric analysis of the device is carried out in terms of DC magnetic field and electron beam parameters such as beam voltage, and beam current to observe the device performance in terms of RF output power and efficiency.

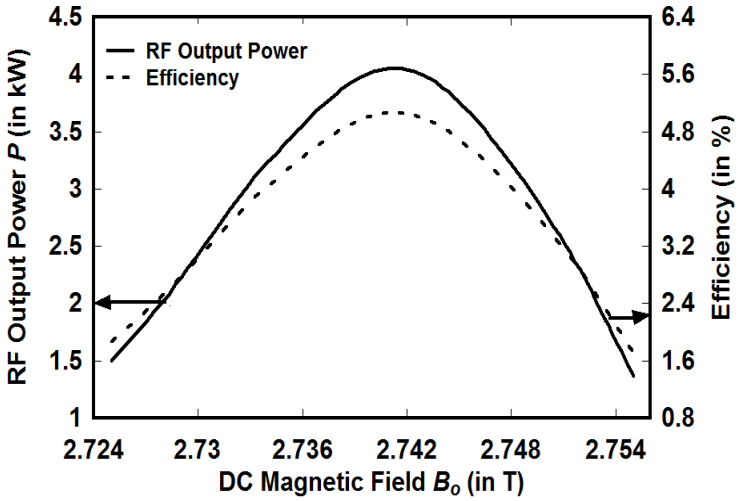

Figure. 4.18: RF output power and efficiency variation with DC magnetic field.

Figure 4.18 shows variation of RF output power and electronic efficiency with DC magnetic field. The energy and the phase bunching phenomenon is directly affected by the difference between the cyclotron frequency and frequency of the EM waves. Since, the cyclotron frequency is decided by the applied DC magnetic field; hence the variation of the static magnetic field has a strong effect on the performance of the device. It is clear from the figure that the 1.03kW peak output power is obtained at the DC magnetic field around 2.74T and sensitive to the variation in DC magnetic field.

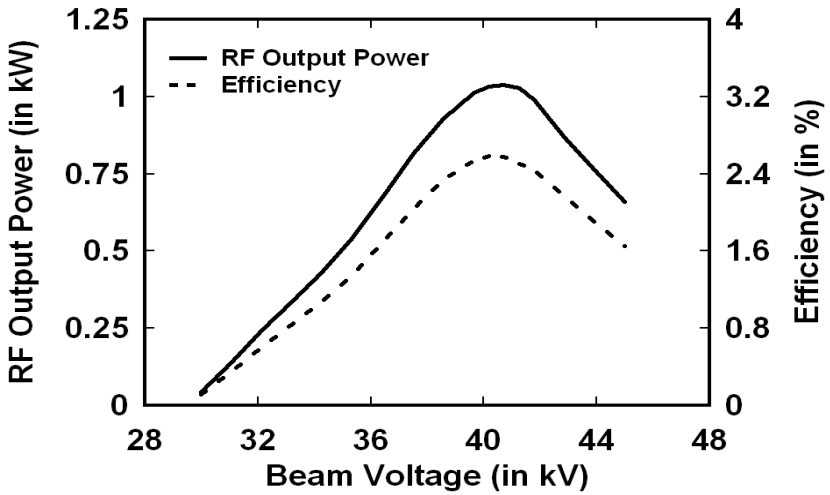

Figure. 4.19: RF output power and efficiency variation with the beam voltage (I_b = 1A, α = 1.5, f_{dr} = 140GHz).

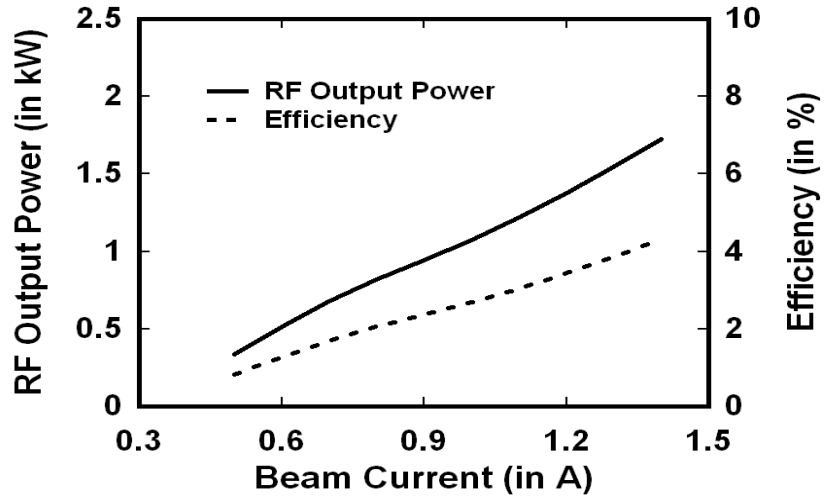

Figure. 4.20: RF output power and efficiency variation with the beam current (V_b = 40kV, α = 1.5).

The variation of RF output power and efficiency with beam voltage is shown in Fig. 4.19. It is observed from the figure that the maximum RF output power around 1.03kW and efficiency around 2.52% is obtained at the beam voltage of 40kV. The dependence of RF output power and efficiency on the beam current is shown in Fig. 4.20 for magnetic field B_0 = 2.74T. From the Fig. it is clear that the RF output power increases with the increase in the beam current which is mainly due to the increase in the beam energy for beam-wave interaction, but the efficiency has a optimum value. Efficiency decrement at higher values

of beam current is mainly due to the degradation of the beam quality due to the over bunching of the electrons. When the beam current exceeds the start oscillation current, the efficiency starts decreasing. The RF output power of 1.03kW with 2.52% electronic efficiency is obtained at the beam current of 1A.

4.7. Conclusion

A detailed design methodology of the second harmonic, cylindrical four-cavity gyroklystron amplifier operating at 140GHz frequency has been developed following analytical approaches. Firstly, essential design constraints for the choice of operating mode are explained. After this, different parameters of the RF section and electron beam such as cavity geometry, drift tube dimensions, beam voltage, beam current, magnetic field, etc. are calculated analytically based on the operating mode, frequency and power. The mode competition is severe problem in the gyroklystron operation and is thoroughly analyzed using start oscillation current criteria. The start oscillation current and coupling coefficient curves also provide us a set of optimized operating parameters, such as, beam current, magnetic field, beam radius, etc., which will excite the desired mode in the resonator cavity. TE_{02} mode has been chosen as the operating mode in each cavity because it ensures the benefit of high coupling coefficient, lower wall loss, feasible cathode design, and an easier design of mode convertor.

Since, the higher frequency and higher harmonic device leads to the problem of mode competition, the developed design methodology has been numerically appreciated by carrying out the time-dependent multimode analysis of the typically selected gyroklystron and has been validated through multimode PIC simulation using a commercial code 'CST Particle Studio'. For the designed parameters, a well above of 1kW of RF output power has

been obtained in the desired TE_{02} mode at 140GHz operating frequency from both the approaches. The device efficiency and gain are obtained as ~2.58% and ~30.13dB respectively. The analytical results and PIC simulation results are found in close agreement ~ 5%. Sensitivity analysis has also been carried out to make the present study of more practical useful.